Synthetic Aperture Radar - Hardware Development

Vilmos RÖSNER[1], *Rudolf SELLER*[1], *Levente DUDÁS*[1], *Károly KAZI*[2], *Gyula MIKÓ*[2]

[1] Dept. of Broadband Infocommunications and Electromagnetic Theory, Budapest University of Technology and Economics, Goldmann Sq. 3., 1111 Budapest, Hungary
[2] Bonn Hungary Electronics Ltd, Hungary

rosner@mht.bme.hu, seller@mht.bme.hu, dudas@mht.bme.hu, kazik@bhe-mw.eu

Abstract. *Experimental real and synthetic aperture radar are developed from the base-band digital unit to the analogue RF parts, based on solid state units, using pulse compression for radar imaging. Proper QPSK code is found for matched filter.*

Keywords

Spread spectrum, matched filter, radar, microwave imaging, SLAR, SAR.

1. Introduction

The conventional radar transmits a short high power pulse and receives the reflected signal. Because of the kW..MW pulse, electron tube is necessary for the power amplifier.

If the transmitted signal is not a simple pulse, but it consists of submodulation, the peak power of the radar can be reduced. In this case, the receiver is a matched filter (correlation receiver) – see Fig. 1.

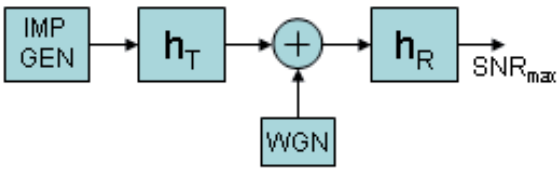

Fig. 1. The correlation receiver.

In order to obtain the maximal signal to noise ratio on the receiver output, the matched filter of the receiver should be the reverse and complex conjugate of transmitter filter (where T is the sub-pulse time, N is the number of the sub-pulses). If the noise of the radio channel is additive white Gaussian-noise, the maximal SNR on the output depends on the energy and not on the power of the transmitted signal – (1, 2, 3).

$$H_{R,opt}(f) = H_T^*(f) \Leftrightarrow h_{R,opt}(t) = h_T^*(N \cdot T - t), \quad (1)$$

$$SNR_{\max} = \frac{2 \cdot E}{N_0}, \quad (2)$$

$$E = \int_0^{N \cdot T} x^2(t)dt. \quad (3)$$

The digital representation of the matched filter with FIR filter is on (4, 5).

$$y(n) = \sum_{k=0}^{N-1} c(k) \cdot x(n-k), \quad (4)$$

$$c(k) := x^*(N-k). \quad (5)$$

In practice, the transmitted pulse is angle modulated signal, because its amplitude is constant in time so the energy is maximal unlike AM or OFDM signal. To analyze and qualify the transmitted pulses, the autocorrelation function has to be used – (6).

$$R(\tau) = \int_{-\infty}^{+\infty} x\left(t + \frac{\tau}{2}\right) \cdot x^*\left(t - \frac{\tau}{2}\right) dt. \quad (6)$$

In sampled case the autocorrelation is the following

$$R(iT) = \sum_{k=-N+1}^{N-1} x(kT) \cdot x^*(iT - kT). \quad (7)$$

2. Code Generation

If the desired "peak power" is 1 kW (in case of the conventional radar), and the transmitted signal is 32 samples long sub-modulated BPSK signal, the average power of the pulse compressed signal is less than 32 W. The dynamic of the receiver depends on the shape of correlation function belongs to the transmitted BPSK signal. The aim is, the autocorrelation function has to be similar to Dirac-pulse, with the minimal peak sidelobe level (PSL).

Code seeker software was developed; its flow chart is in Fig. 2. It generates B/QPSK code series according to pseudo-random number generator with white probability distribution, and calculates the PSL of its autocorrelation function. If PSL is greater than 20 dB, the code is written to file, else it generates another code series.

Because of the calculation of the correlation function, the code seeker software on PC is too slow (it is about one proper code/hour). It was necessary to develop hardware

accelerator, which was based on FPGA. Achieved acceleration rate is about 30 dB. This hardware is in Fig. 3. Using code seeker program, about a day is necessary to find a proper code set but with the code seeker hardware, this time is less than 2 minutes.

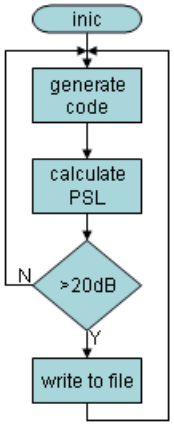

Fig. 2. The code seeker software.

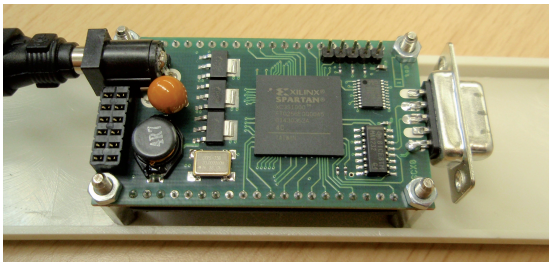

Fig. 3. The code seeker hardware.

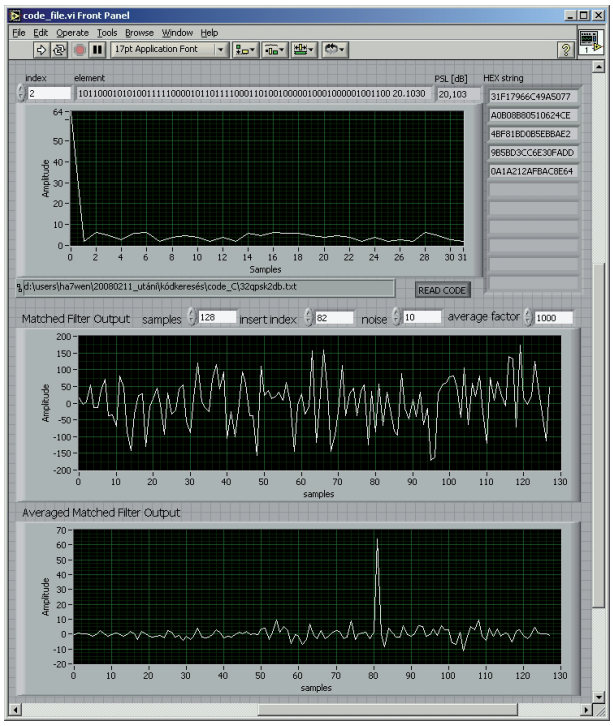

Fig. 4. The channel simulation.

We made the channel simulation software, see Fig. 4. Used the generated PSK codes, the software models the effect of the additive Gaussian white noise. If the PSL is e.g. 20 dB, the noisy signal can be received by the matched filter about 20 dB under the noise level.

3. SAR Hardware

The block scheme of the SAR hardware is in Fig. 5. The digital FPGA and DSP unit generates the output QPSK signal in intermediate frequency. This signal is converted up to the RF band with a synthesizer and a mixer and amplified to an appropriate power level.

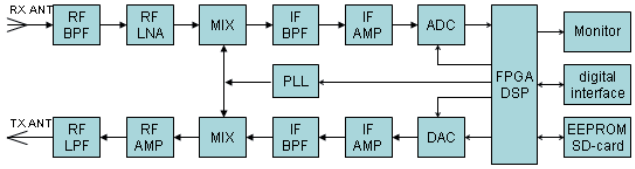

Fig. 5. The block scheme of the hardware.

The reflected signal is received and converted down to the IF band, and digitalized by ADC. The matched filter is digitally realized in FPGA. The received IQ-signal is saved to a high capacity high speed EEPROM (SD card). The picture of the hardware can be seen in Fig. 6, and its high-power amplifier in Fig. 7. The phase stability of the HPA during the pulse length is critical for the spread spectrum modulation technique.

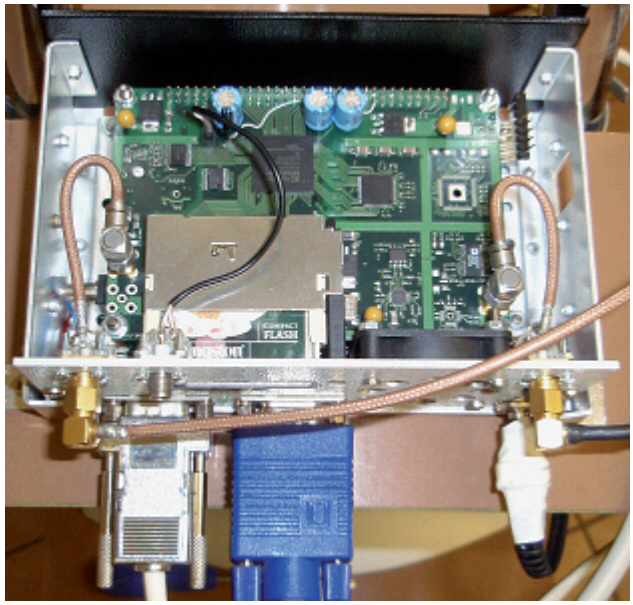

Fig 6. The SAR hardware.

This SAR hardware is able to record the baseband digital I-Q data – reflected from the environment – using high-speed digital signal processing with digital IF unit.

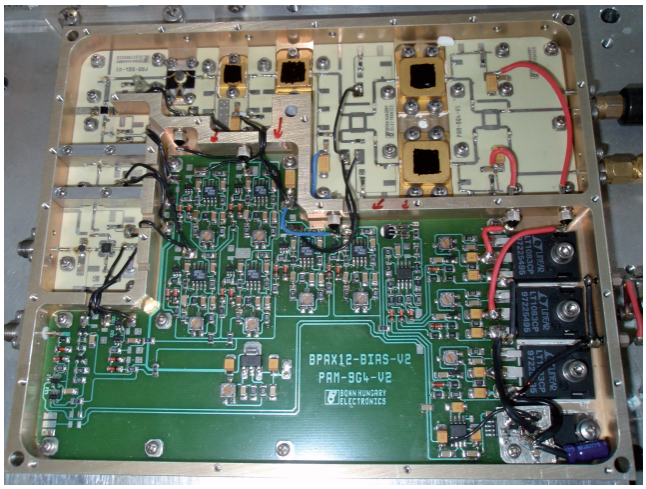

Fig. 7. HPA unit.

4. Laboratory Measurements Results

In our laboratory, we made an experimental arrangement – see Fig. 8 (HPA was not used, because of short distance). You can see the SAR hardware, the transmitter and receiver antennas and monitor to show the reflected and received base-band signals on the output of the matched filter.

Fig. 8. The indoor measurement.

If CW signal is transmitted, the RF spectrum is the following – Fig. 9. If unmodulated pulse is used, the output spectrum is similar to sinc function – see Fig. 10. If we use 32 sub-pulses length QPSK code modulated signal, the output signal is similar to wideband noise – see Fig. 11. If we moved a corner reflector in front of the radar, the received base-band signal is in Fig. 12. You can see in this picture, the waterfall, which shows a target moving away.

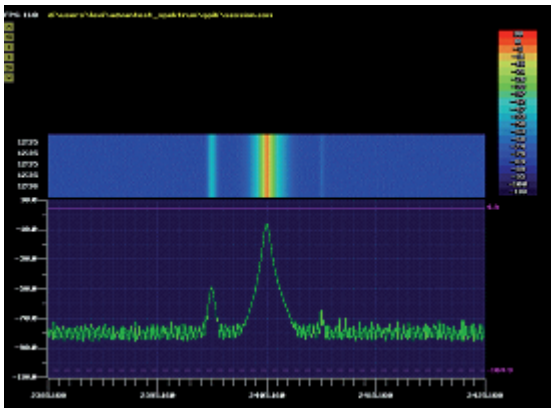

Fig. 9. The CW signal.

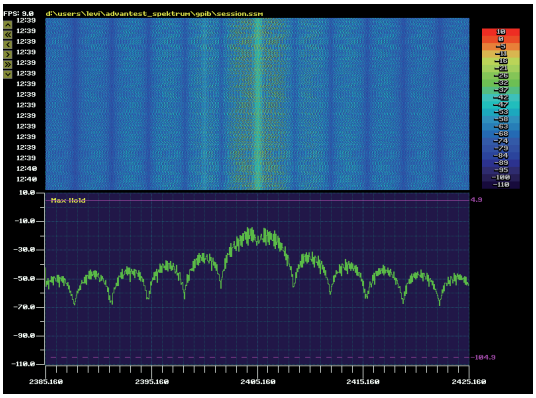

Fig. 10. The spectrum of a simple pulse.

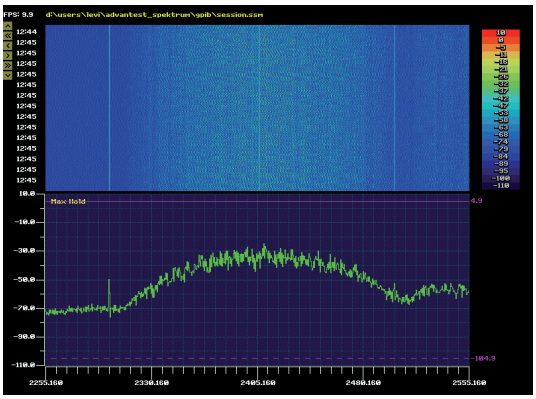

Fig. 11. The code modulated signal in frequency domain.

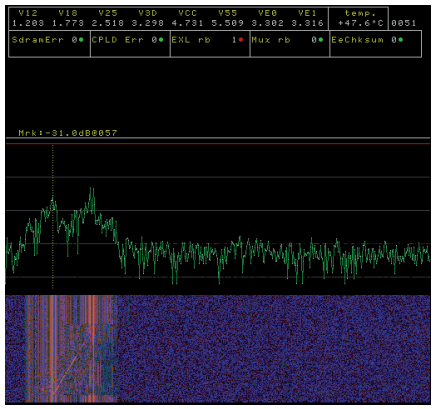

Fig. 12. The matched filter output in time domain.

5. Flight Measurement Using Real Aperture (SLAR) Evaluation Mode

The first test measurements were done from the top of our building, mounting the SLAR on a pan-and-tilt, with tilting disabled. Some main streets and flats were identified on the image, however, the very low altitude and looking angle prevented us from acquiring a good image (urban environment is also not a good test site, as the houses are too frequently spaced, shadowing each other, thus the image of a city even from above has few details.) The test demonstrated the abilities well, however. For the flight measurements the SLAR equipment, with a 3 meters long antenna, was mounted on a MI-17 military transport helicopter (Fig. 13). The antenna's 3 dB beam width is about 0.6 degrees.

The test flights were done in the area of Szolnok, Hungary, at an altitude of 500-1000 meters. The backdraw of the helicopter flight is that the aircraft had an oscillating motion around its yaw axis. The effect of this can be seen on the images, as straight lines become curly. This should be less of a problem on the proposed unmanned aerial vehicle (UAV). Also, the availability of navigational data synchronized with the SLAR/SAR data should help in geometric corrections.

Fig. 13. SLAR equipment on a helicopter.

Open water surfaces, like the river Tisza can easily be distinguished on SLAR images. Being nearly homogeneous planes (compared to the wavelength), they reflect almost no backscattered energy to the antenna, making their image black on the grayscale result (it needs high spatial frequency water waves to cause a significant reflection). Agricultural fields are relatively flat and thus also produce little reflection, but still can be seen because the soil roughness is comparable to the wavelength.

Even different types of fields can be distinguished. Vegetation scatters waves in every direction. Groups of trees look similar to small hills, projecting a shadow. (There are a few groups near the rivers.) Railroads and roads can be identified easily when they are running on dykes (this happens often in the flood-basin), and can disappear when running on flat lands (railroads have more chance due to their structure not being plane). The banks of the river Tisza are steep here, and thus make a bright reflection when they are perpendicular to the flight path (on the image below, the aircraft flew on the left side, thus the right bank of the river can best be seen. The railroad bridge on the lower part of the image also produces a bright reflection. The village of Szajol (near Szolnok) can be seen in the middle-right part as a somewhat chaotic dump of bright dots.

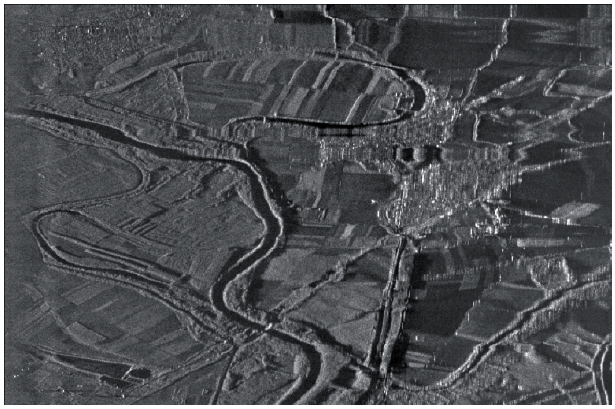

Fig. 14. Our SLAR image of the town of Szajol (near Szolnok) and the Tisza river.

Fig. 15. The same area on satellite image (optical).

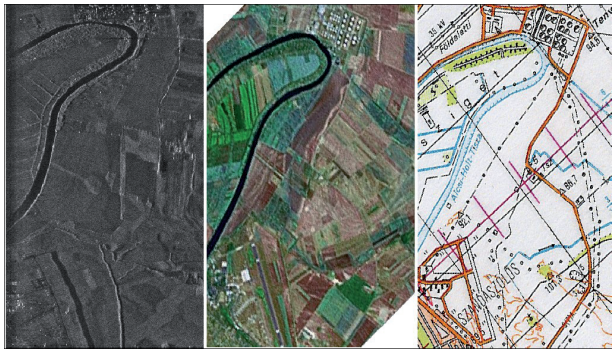

Fig. 16. Comparison of different terrain features on SLAR image, optical image and map.

Test flights have shown that it is fully functional, realizing the 10x10 meters resolution. To achieve better resolution, it demands a longer antenna. But we are not able to increase the size of the antenna because of mechanical reasons. Instead of it, we use another signal proc-

essing algorithm called synthetic aperture radar imaging, so we realize the longer antenna in time. In this way, we upgrade our SLAR into a SAR. The device was developed from the beginning to contain I-Q receivers, coherent with the transmitter, making the upgrade easier. SAR operation needs significantly more data processing and storage capabilities than SLAR mode, thus an upgrade is necessary in the DSP unit with inclusion of a compact flash memory unit and a fast data interface. The creation of the SAR image from the gathered data (that is, the aperture synthesis) is done after the flight, on laboratory PCs. Writing the synthesis software is also a part of the development.

6. Site Measurement Using Synthetic Aperture (SAR) Evaluation Mode

The flight by a helicopter is not capable in SAR mode because of the trajectory instability. We have to develop the trajectory error compensation system using gyroscope sensor, accelerometer and GPS. This development is in progress, simplified measurement arrangement was chosen to prove the SAR evaluation method.

Instead of a helicopter, the SAR hardware and the antennas are mounted on a car – see Fig. 17. The SAR method does not need a long antenna, in practical point of view, two simple horn antennas were used.

Fig. 17. SAR equipment on a car.

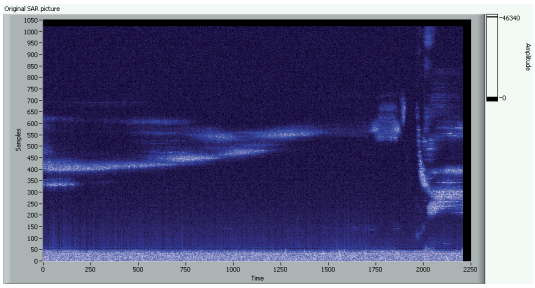

Fig. 18. The raw SAR picture.

Our first measurements were made in an unused airfield, by mounting the radar antenna on top of a car – Fig. 17. The saved raw IQ samples is in Fig. 18.

To decrease coupling between transmitter and receiver chains two antennas were used. It also results in a decrease of minimal range, (in mono-static radars the long sub-modulated pulses result in a long minimal detection distance). The bandwidth of the pulse compression was 100 MHz resulting in an in-range resolution of $c/2B = 1.5$ meters. In the azimuth direction samples are integrated such that resulting samples are taken about every 0.5 meters (at 20 Hz and about 10 m/s). These values are optimized for the car-mounted test, and will be different for an airplane (which can only go faster). The processing software corrects the results to have 1.5 m by 1.5 m resolution.

We have set up a corner reflector at about 100 meters from the runway and driven the car at moderate speed (40..60 km/h) for about 2 km. In the images the reflector can be clearly seen with the sidelobes in both directions. In the range direction the sidelobes come from the pulse compression (the correlation function), in the flight direction they come from the aperture synthesis (sidelobes of the antenna array's gain pattern). With proper image contrast settings these sidelobes are barely seen. We have enhanced them for testing purposes on most of the images shown here. The airfield was bounded by a long patch of forest and inclined land that can be seen at the edge of the image.

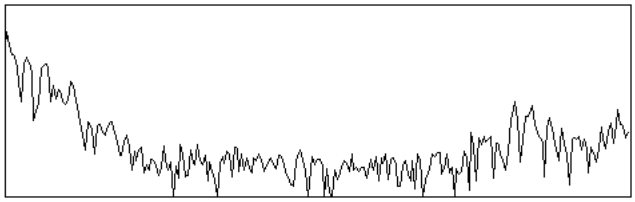

Fig. 18. One row of raw data (time domain).

Fig. 19. Left: unprocessed image part. The raw image of point-like targets is an outward curved arc (plus the correlation sidelobes if pulse compression is used). Middle and right: the same area after processing. This is the image of a corner reflector. The image at the right has different contrast enhancement to show the time domain sidelobes (from the correlation) in the vertical direction and the aperture synthesis sidelobes in the horizontal direction.

7. Conclusions

The developed real and synthetic aperture radars are good working order, we measured the hardware in our laboratory and in real environment. It can record the baseband samples for the further SAR imaging. Novelties of this hardware and signal processing are:

- Wideband (B=100MHz)
- Spread spectral waveform generation
- Real-time matched filter for the 100 MHz signal
- 30 W high-duty microwave power amplifier
- High data-rate archive unit
- Holographic image generation

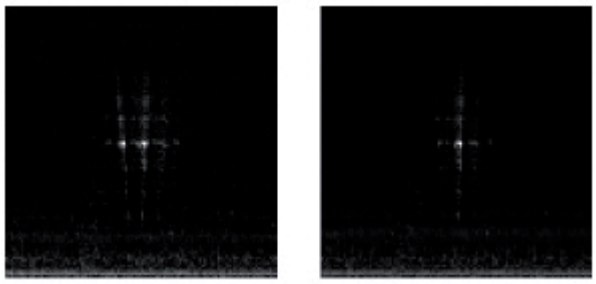

Fig. 20. The same area processed with applying a rectangular window function (left) and a Hann-window (right). Using non-rectangular window functions decreases the artifacts (sidelobes) from the image processing.

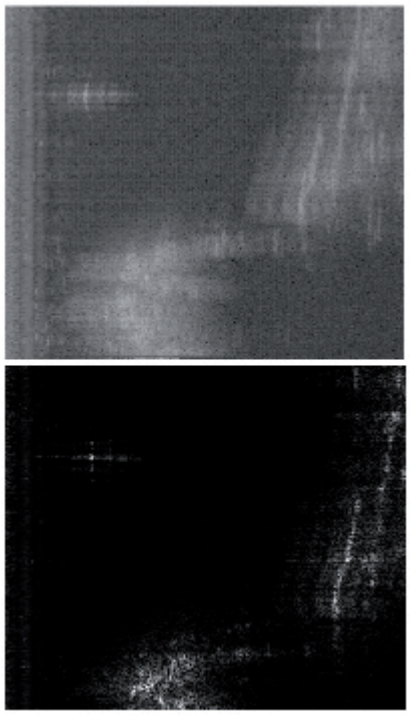

Fig. 21. Upper: raw image. Lower: Processed image. The corner reflector is on the left upper side, the forest line is on the right side.

Future work will include realizing a higher carrier and modulating frequency; integrating GPS and orientation sensors for navigational data acquisition. We are also working on adapting commercial radar image processing software to our radar format and also on upgrading our own processing software. Future measurements will have to be made from airplanes to show the true potential of the radar. Further important point of view is the minimization of the size and mass for the small-sized UAV application.

Acknowledgement

NKTH
National Office for Research and Technology
Established by the support of the National Office for Research and Technology.

References

[1] ULABY, F. T., et al. *Microwave Remote Sensing*. Addison-Wesley Publishing Company, 1981.

[2] BARTON, K. B. *Modern Radar System Analysis*. Artech House, 1988

[3] OLIVER, C., QUEGAN, S. *Understanding Synthetic Aperture Radar Images*. Artech House.

[4] CURLANDER, J. C., MCDONOUGH, R. N. *Synthetic Aperture Radar: Systems and Signal Processing.* Wiley Series in Remote Sensing and Image Processing ISBN 0-471-85770-X

[5] MEHRDAD SOUMEKH *MATLAB & Simulink Based Books-Signal Processing Synthetic Aperture Radar Signal Processing with MATLAB Algorithms.* John Wiley & Sons, Inc., 1999 ISBN 0-471-29706-2

[6] BASSEM MAHAFZA *Radar Signal Analysis and Processing Using MATLAB.* CRC Press, 2008. ISBN 9781420066432

[7] DALL, J. A fast autofocus algorithm for synthetic aperture radar processing. In Acoustics, Speech, and Signal Processing, 1992. ICASSP-92. 1992 IEEE International Conference. vol. 3, p. 5 – 8.

[8] ULANDER, L. M. H., HELLSTEN, H., STENSTROM, G. Synthetic-aperture radar processing using fast factorized back-projection. *IEEE Transactions on Aerospace and Electronic Systems,* July 2003, vol. 39, no. 3, p. 760- 776.

About Authors...

Rudolf SELLER received MSc. degree from Budapest University of Technology and Economics in 1987 at the Faculty of Electrical Engineering and Informatics. He received his Dr. degree in 1996. His research interests include antennas, antenna related signal processing, microwave imaging, radar signal processing, and adaptive space-time signal processing.

Levente DUDÁS was born in Budapest, Hungary. He graduated from Budapest University of Technology and Economics in 2007 at the Faculty of Electrical Engineering and Informatics, receiving MSc. degree. He has been a Ph.D. student since 2007, focusing on antenna systems, RF and radar technologies.